

Modulation of single-chain-magnet behaviour in a heterometallic Fe₂Co cyanide bridged 2D sheet

Ranjan Kharel, Jyoti Yadav, Sanjit Konar*

Department of Chemistry, Indian Institute of Science Education and Research Bhopal, Bhauri, Bhopal By-pass Road, Madhya Pradesh, India- 462066.
E-mail: skonar@iiserb.ac.in

Contents

1. Experimental Procedure
2. Physical measurements
3. Result and discussion

1. Experimental Procedure

The cyanide building unit Na[FeTp(CN)₃] and the ligand (*E*)-1,2-bis(4-(1H-imidazol-1-yl)phenyl)diazene were prepared according to the previously reported procedures.¹⁻⁴ The compound **1·3.5H₂O** and **2** were prepared as described below.

1.1. Synthesis of Complex **1·3.5H₂O**

3 mL aqueous solution of Co(BF₄)₂·6H₂O (0.01 mmol) was taken in a test tube and layered over with 3 mL methanolic solution of Na[FeTp(CN)₃] (0.02mmol) and (*E*)-1,2-bis(4-(1H-imidazol-1-yl)phenyl)diazene (0.01 mmol) using 3mL buffer solution of MeOH/H₂O (1:1, v/v). The test tube was left undisturbed for two weeks to obtain red crystals of the complex.

IR (cm⁻¹): $\nu_{\text{CN}} = 2124, 2162$ (broad) cm⁻¹ and $\nu_{\text{BH}} = 2483, 2499$ cm⁻¹

1.2. Synthesis of Complex **2**

3 mL aqueous solution of Zn(BF₄)₂·6H₂O (0.01 mmol) was taken in a test tube and layered over with 3 mL methanolic solution of Na[FeTp(CN)₃] (0.02mmol) and (*E*)-1,2-bis(4-(1H-imidazol-1-yl)phenyl)diazene (0.01 mmol) using 3mL buffer solution of MeOH/H₂O (1:1, v/v). The test tube was left undisturbed for two weeks to obtain red crystals of the complex.

IR (cm⁻¹): $\nu_{\text{CN}} = 2162, 2122$ and 2076 cm⁻¹ and $\nu_{\text{BH}} = 2490$ cm⁻¹ (broad).

Elemental Analysis

For Complex **1·3.5H₂O**: (Experimental): C = 43.91%, H = 3.38% and N = 29.40%; Calculated: C = 44.63%, H = 3.66% and N = 29.74%.

For Complex **1**: (Experimental): C = 46.82%, H = 3.28% and N = 30.63%; Calculated: C = 47.27%, H = 3.21% and N = 31.50%.

For Complex **2**: (Experimental): C = 44.59%, H = 3.63 % and N = 29.90%; Calculated: C = 44.34%, H = 3.63% and N = 29.20%.

2. Physical measurements

2.1. Energy Dispersive X-Ray (EDX) spectrometer

The EDX data were recorded on a 50 mm² Silicon drift detector which has an Mn-K α resolution of 127 eV controlled by INCA (Integrated Calibration and Application Tool) software.

2.2. FT-Infrared Spectroscopy

FT-IR spectra were measured by using a Perkin-Elmer Spectrum BX Spectrometer with a wavenumber ranging between 4000 cm⁻¹ - 400 cm⁻¹.

2.3. UV-Visible Spectroscopy

The solid phase UV-visible spectroscopic data was collected using Cary 100 instrument using Scan Software Version 4.20(468) scanning between wavelengths 200 nm to 1200 nm.

2.4. Powder XRD

Powder X-ray diffraction (PXRD) data were collected on a PANalytical EMPYREAN instrument using Cu K α radiation.

2.5. Single Crystal X-ray Diffraction

Intensity data were collected on a 'Bruker D8-Venture' diffractometer using a graphite monochromated Mo-K α radiation ($\lambda = 0.71073$) and Cu- K α ($\lambda = 1.54178$) at different temperatures. Data collections were performed using ϕ and ω scan.^{5,6} Olex2 was used as the graphical interface and the structures were solved with olex2.solve structure solution program using Charge Flipping and refined with the ShelXT refinement package using Least-Squares minimisation.^{5,6} All non- hydrogen atoms were refined anisotropically.

2.6. Magnetic measurement

The magnetic study has been performed using a SQUID-VSM magnetometer. All samples were ground properly before measuring magnetic moment vs. temperature data, to minimize the reorientation of the crystalline particles under the applied DC field. The measurements have been performed at various applied DC fields in the temperature range of 2-300 K. The measured values were corrected for the experimentally measured contribution of the sample holder, and the derived susceptibilities were corrected for the diamagnetism contribution of the samples, estimated from Pascal's tables.

2.7. Thermogravimetric Analysis

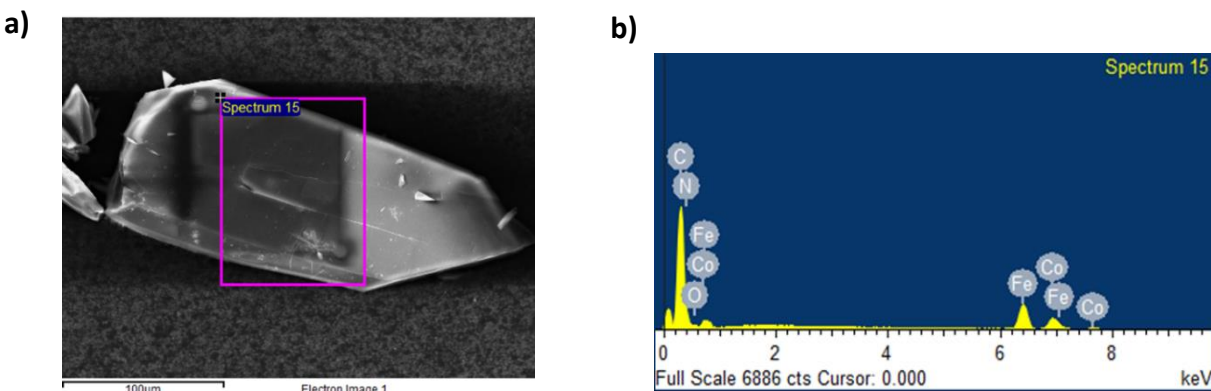
The Thermogravimetric Analysis was performed on a PerkinElmer instrument at a scan rate of 5 K/min, under dry N₂ atmosphere.

2.8. Mössbauer Studies

⁵⁷Fe Mossbauer measurements were carried out in transmission mode with ⁵⁷Co radioactive source in constant acceleration mode using standard PC-based Mossbauer spectrometer equipped with Wissel velocity drive. Velocity calibration of the spectrometer was done with natural iron absorber at room temperature. Sample was mounted in Janis make cryostat for low temperature measurements. The spectra was analysed with NORMOS program.

3. Result and Discussions

3.1. EDX:



Element	Weight%	Atomic%
C K	51.75	62.43
N K	28.35	29.33
O K	4.89	4.43
Co K	5.20	1.28
Fe K	9.80	2.54
Totals	100.00	

Figure S1. EDX (elemental contents) of complex **1·3.5H₂O**

3.2. Infrared spectroscopy:

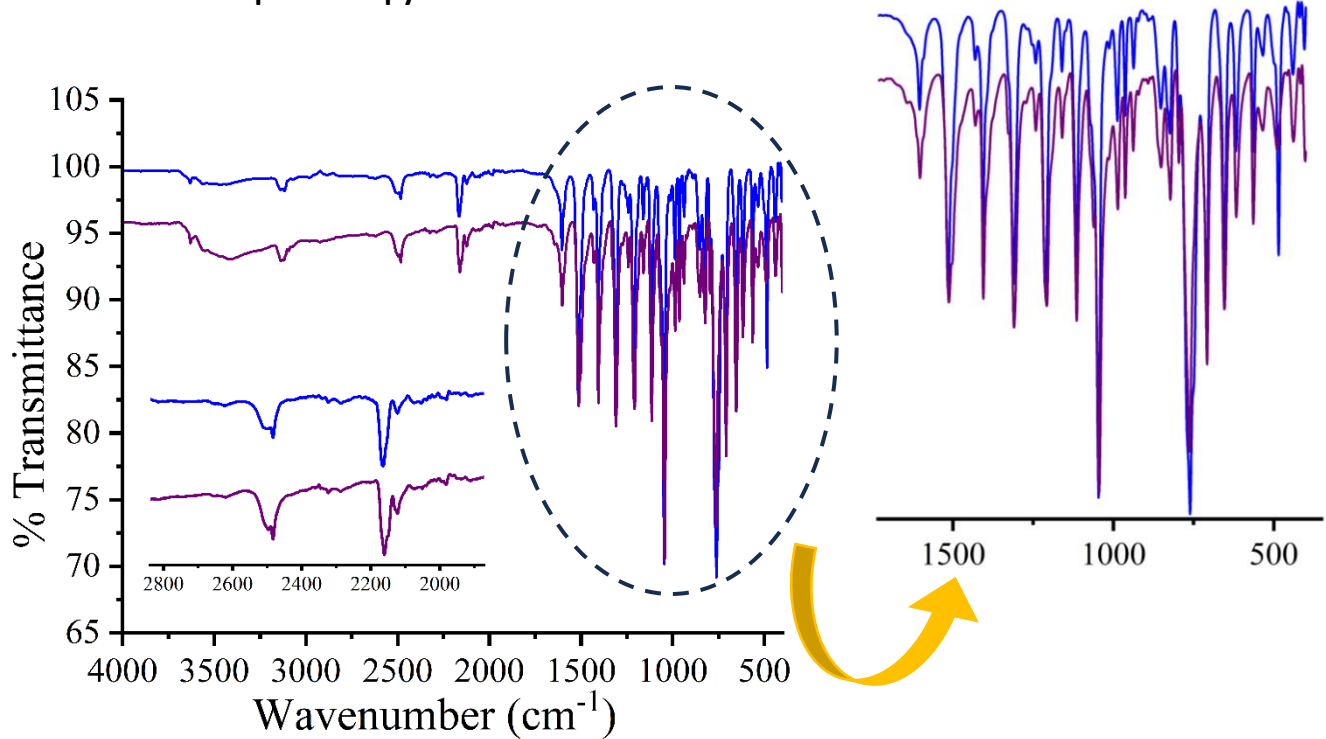


Figure S2: FT-IR spectra of crystal obtained through layer-by-layer technique (purple) and product obtained on direct mixing (blue). Inset indicates identical ν_{CN} peaks ($2100-2200 \text{ cm}^{-1}$) and ν_{BH} peaks for both the samples. The identical spectra in the fingerprint region confirm that the products are identical.

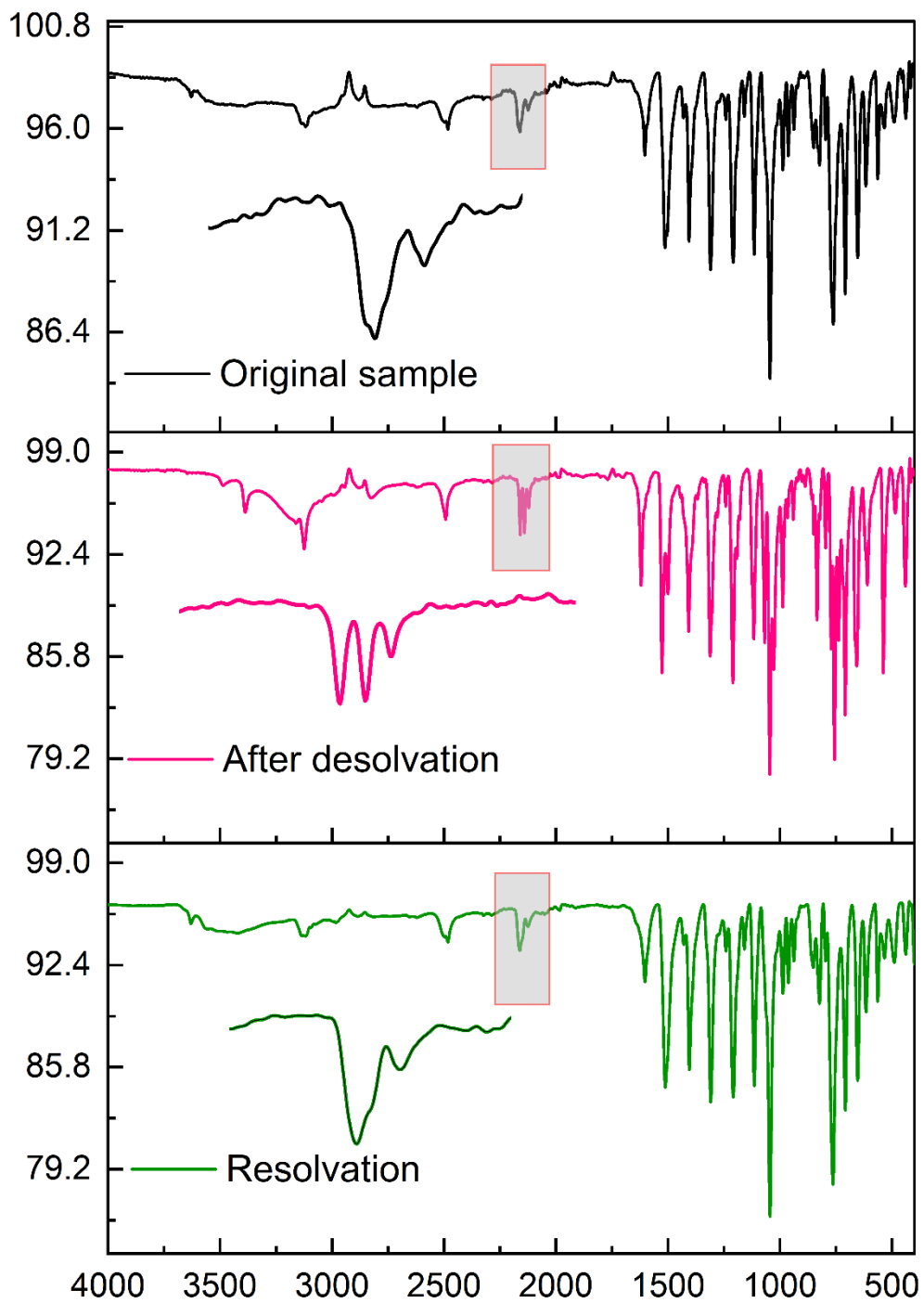


Figure S3: FT-IR for **1**·3.5H₂O at 300 K, Inset shows the change in ν_{CN} stretching frequency. The broad cyanide peaks as highlighted are well resolved after removal of the water molecules and on subjecting to water for a day, the original spectrum is regained. The two bands at 2160 and 2124 cm⁻¹ corresponding to the bridging ν_{CN} of [Fe^{III}_{LS}(μ-CN)Co^{II}_{HS}] linkages and terminal cyanide of [FeTp(CN)₃]⁻ units respectively.

3.3. UV-Vis spectroscopy:

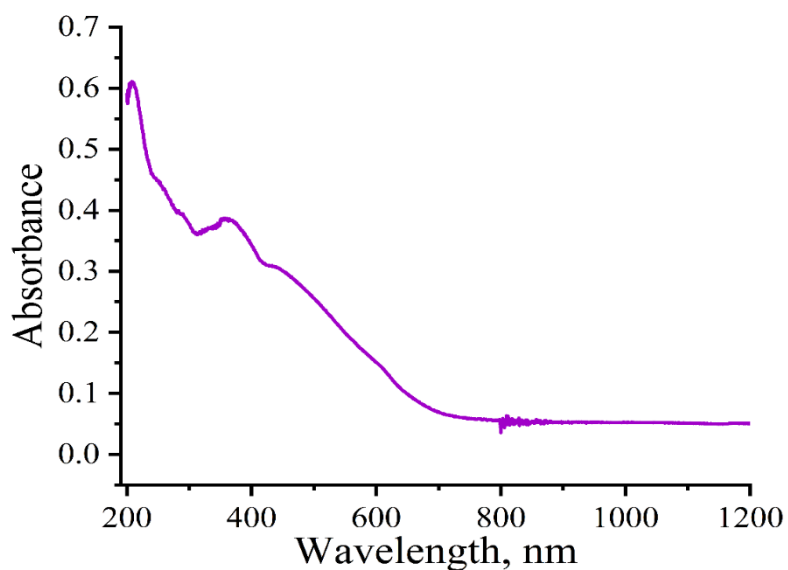


Figure S4: Solid-state UV-Vis-NIR absorption spectra for **1**· $3.5\text{H}_2\text{O}$ at 300 K. The band at 438 nm, stands for the metal-to-metal charge transfer (MMCT) from $\text{Co}^{\text{II}}_{\text{HS}}$ to $\text{Fe}^{\text{III}}_{\text{LS}}$, thus confirming the presence of only paramagnetic $\{\text{Fe}^{\text{III}}_{\text{LS}}(\mu\text{-CN})\text{Co}^{\text{II}}_{\text{HS}}\}$ units in the chain at 300 K.

3.4. Powder XRD:

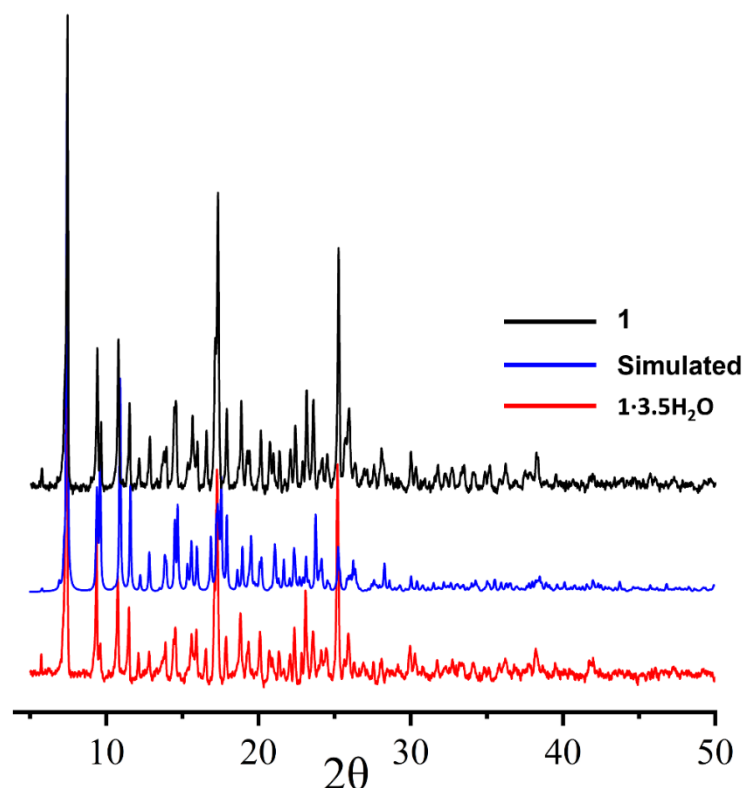


Figure S5: Powder X-ray diffraction pattern of **1**· $3.5\text{H}_2\text{O}$ and **1**. Black and red lines represent the experimental values, and the blue line represents the calculated pattern from the SC-XRD data.

3.5. Structural details:

Table S1. The unit cell and refinement parameters of complexes **1**·3.5H₂O (103 K, 245 K), **1** and **2** (100 K).

Complex	1·3.5H ₂ O		1	2
Temperature/ K	103 K	245 K	100 K	100 K
Identification code	Complex-1_103K	Complex-1_245K	Complex-1_desol	Complex-2_Zn
CCDC No.	2270783	2270789	2270788	2270790
Empirical formula	C ₄₂ H _{35.7} B ₂ CoFe ₂ N ₂₄ O _{3.5}	C ₄₂ H ₃₃ B ₂ CoFe ₂ N ₂₄ O _{3.5}	C ₄₂ H ₃₄ B ₂ CoFe ₂ N ₂₄	C _{42.5} H _{38.5} B ₂ Fe ₂ N ₂₄ O ₄ Zn
Formula weight	1124.92	1122.17	1067.18	1148.16
Crystal system	triclinic	triclinic	triclinic	triclinic
Space group	P-1	P-1	P-1	P-1
a/Å	12.176(4)	12.328(6)	11.9253(7)	12.3580(4)
b/Å	13.726(4)	13.811(7)	13.8081(8)	13.8278(5)
c/Å	16.323(5)	16.391(8)	16.3778(9)	13.8278(5)
α/°	68.781(9)	68.709(14)	68.189(3)	68.011(2)
β/°	86.578(10)	86.925(15)	86.117(4)	86.398(2)
γ/°	79.806(10)	79.548(16)	80.393(4)	78.696(2)
Volume/Å ³	2502.9(14)	2557(2)	2468.6(3)	2556.72(15)
Z	2	2	2	2
ρ _{calc} g/cm ³	1.493	1.458	1.436	1.491
μ/mm ⁻¹	0.966	0.946	7.732	5.600
F(000)	1145.0	1140.0	1086.0	1171.0
Crystal size/mm ³	0.23 × 0.12 × 0.07	0.23 × 0.12 × 0.07	0.27 × 0.15 × 0.09	0.25 × 0.13 × 0.09
Radiation	MoKα (λ = 0.71073)	MoKα (λ = 0.71073)	CuKα (λ = 1.54178)	CuKα (λ = 1.54178)
2Θ range for data collection/°	4.402 to 53.516	4.86 to 53.03	5.812 to 127.974	7.016 to 133.674
Index ranges	-15 ≤ h ≤ 15, -17 ≤ k ≤ 17, -20 ≤ l ≤ 20	-15 ≤ h ≤ 15, -17 ≤ k ≤ 17, -20 ≤ l ≤ 20	-13 ≤ h ≤ 13, -16 ≤ k ≤ 16, -19 ≤ l ≤ 19	-14 ≤ h ≤ 14, -16 ≤ k ≤ 16, -18 ≤ l ≤ 19
Reflections collected	31092	40692	51522	111544
Independent reflections	10307 [R _{int} = 0.1160, R _{sigma} = 0.1473]	10538 [R _{int} = 0.1141, R _{sigma} = 0.1175]	7905 [R _{int} = 0.0943, R _{sigma} = 0.0618]	8958 [R _{int} = 0.0618, R _{sigma} = 0.0275]
Data/restraints/parameters	10307/0/722	10538/0/747	7905/0/643	8958/0/751
Goodness-of-fit on F ²	0.980	0.988	1.052	1.060
Final R indexes [I>=2σ (I)]	R ₁ = 0.0691, wR ₂ = 0.1502	R ₁ = 0.0626, wR ₂ = 0.1385	R ₁ = 0.0459, wR ₂ = 0.1037	R ₁ = 0.0469, wR ₂ = 0.1135
Final R indexes [all data]	R ₁ = 0.1434, wR ₂ = 0.1890	R ₁ = 0.1331, wR ₂ = 0.1736	R ₁ = 0.0673, wR ₂ = 0.1130	R ₁ = 0.0522, wR ₂ = 0.1162

Table S2. Selected bond lengths (\AA) and angles ($^\circ$) of complexes **1**·3.5H₂O (103 K, 245 K), **1** and **2** (100 K).

Complex-1_103K			
Bond Length (Å)			
Co1-N9 ⁴	2.080(5)	Fe1-N1	1.972(5)
Co1-N9	2.080(5)	Fe1-N3	1.974(5)
Co1-N18 ⁵	2.091(5)	Fe1-N5	1.954(5)
Co1-N18 ⁶	2.091(5)	Fe1-C12	1.901(7)
Co1-N10	2.092(5)	Fe1-C10	1.893(6)
Co1-N10 ⁴	2.092(5)	Fe1-C11	1.924(7)
Co2-N7 ¹	2.115(5)	Fe2-N21	1.975(5)
Co2-N7 ²	2.115(5)	Fe2-N19	1.963(5)
Co2-N16	2.064(5)	Fe2-N23	1.962(5)
Co2-N16 ³	2.064(5)	Fe2-C33	1.903(7)
Co2-N15	2.072(5)	Fe2-C31	1.930(6)
Co2-N15 ³	2.072(5)	Fe2-C32	1.924(7)
Bond Angle (°)			
N9-Co1-N9 ⁴	180.0	N1-Fe1-N3	88.5(2)
N9-Co1-N18 ⁵	88.61(19)	N5-Fe1-N1	88.0(2)
N9 ⁴ -Co1-N18 ⁶	88.61(19)	N5-Fe1-N3	88.47(19)
N9-Co1-N18 ⁶	91.39(19)	C12-Fe1-N1	178.0(2)
N9 ⁴ -Co1-N18 ⁵	91.39(19)	C12-Fe1-N3	89.6(2)
N9 ⁴ -Co1-N10 ⁴	90.63(19)	C12-Fe1-N5	91.1(2)
N9-Co1-N10 ⁴	89.37(19)	C12-Fe1-C11	90.2(3)
N9 ⁴ Co1N10	89.37(19)	C10-Fe1-N1	97.6(2)
N9Co1N10	90.63(19)	C10-Fe1-N3	173.7(2)
N18 ⁵ Co1N18 ⁶	180.0(3)	C10-Fe1-N5	90.5(2)
N18 ⁶ Co1N10 ⁴	89.62(19)	C10-Fe1-C12	84.2(2)
N18 ⁵ Co1N10 ⁴	90.38(19)	C10-Fe1-C11	89.4(2)
N18 ⁶ Co1N10	90.38(19)	C11-Fe1-N1	90.7(2)
N18 ⁵ Co1N10	89.62(19)	C11-Fe1-N3	91.7(2)
N10 ⁴ Co1N10	180.0	C11-Fe1-N5	178.7(3)
N7 ¹ -Co2-N7 ²	180.0	N19-Fe2-N21	87.9(2)
N16-Co2-N7 ²	87.32(18)	N23-Fe2-N21	88.5(2)
N16 ³ -Co2-N7 ²	92.68(18)	N23-Fe2-N19	89.4(2)
N16 ³ -Co2-N7 ¹	87.32(18)	C33-Fe2-N21	92.4(2)
N16-Co2-N7 ¹	92.68(18)	C33-Fe2-N19	92.5(2)
N16 ³ -Co2-N16	180.0	C33-Fe2-N23	177.9(2)
N16-Co2-N15 ³	90.4(3)	C33-Fe2-C31	85.6(3)
N16-Co2-N15	89.5(3)	C33-Fe2-C32	87.7(3)
N16 ³ -Co2-N15 ³	89.5(3)	C31-Fe2-N21	90.9(2)
N16 ³ -Co2-N15	90.5(3)	C31-Fe2-N19	177.7(2)
N15 ³ -Co2-N7 ²	88.7(2)	C31-Fe2-N23	92.5(2)
N15-Co2-N7 ¹	88.7(2)	C32-Fe2-N21	179.9(3)
N15 ³ -Co2-N7 ¹	91.3(2)	C32-Fe2-N19	92.2(2)
N15-Co2-N7 ²	91.3(2)	C32-Fe2-N23	91.4(3)
N15 ³ -Co2-N15	180.00(17)	C32-Fe2-C31	89.1(3)

Complex-1_245K			
Bond Length Å			
Co1-N9 ⁴	2.101(5)	Fe1-N1	1.979(4)
Co1-N9	2.101(5)	Fe1-N3	1.976(4)
Co1-N18 ⁵	2.116(4)	Fe1-N5	1.959(5)
Co1-N18 ⁶	2.116(4)	Fe1-C12	1.900(6)
Co1-N10	2.117(4)	Fe1-C10	1.916(5)
Co1-N10 ⁴	2.117(4)	Fe1-C11	1.915(6)
Co2-N7 ¹	2.138(4)	Fe2-N21	1.976(5)
Co2-N7 ²	2.138(4)	Fe2-N19	1.962(5)
Co2-N16	2.101(5)	Fe2-N23	1.965(4)
Co2-N16 ³	2.101(5)	Fe2-C33	1.912(6)
Co2-N15	2.140(2)	Fe2-C31	1.910(6)
Co2-N15 ³	2.140(2)	Fe2-C32	1.916(6)
Co2-N15A	2.113(14)		
Co2-N15A ³	2.113(15)		
Bond Angle (°)			
N18 ² -Co1-N-18	180.0	N3-Fe1-N1	88.74(17)
N18 ² -Co1 -N10 ⁴	89.81(16)	N5-Fe1 -N1	88.18(18)
N18 -Co1 -N10 ⁴	90.19(16)	N5-Fe1 -N3	88.04(18)
N18 -Co1 -N10 ⁵	89.81(16)	C12 -Fe1 -N1	178.0(2)
N18 ² -Co1 -N10 ⁵	90.19(16)	C12 -Fe1 -N3	89.64(19)
N9 ² -Co1 -N18	91.59(16)	C12 -Fe1 -N5	90.6(2)
N9 -Co1 -N18 ²	91.60(16)	C12 -Fe1 -C10	84.8(2)
N9 -Co1 -N18	88.40(16)	C12 -Fe1 -C11	90.3(2)
N9 ² -Co1 -N18 ²	88.41(16)	C10 -Fe1 -N1	96.83(19)
N9 ² -Co1 -N9	180.0	C10 -Fe1 -N3	174.15(18)
N9 -Co1 -N10 ⁴	89.74(17)	C10 -Fe1 -N5	90.33(19)
N9 -Co1 -N10 ⁵	90.26(17)	C11 -Fe1 -N1	90.9(2)
N9 ² -Co1 -N10 ⁵	89.74(17)	C11 -Fe1 -N3	92.0(2)
N9 ² -Co1 -N10 ⁴	90.26(17)	C11 -Fe1 -N5	179.1(2)
N10 ⁴ -Co1 -N10 ⁵	180.0	C11 -Fe1 -C10	89.7(2)
N7 ¹ -Co2 -N7 ²	180.00(7)	N23-Fe2 -N21	88.12(17)
N7 ¹ -Co2 -N15 ³	93.9(5)	N19-Fe2 -N23	89.41(18)
N7 ¹ -Co2 -N15	86.1(5)	N19-Fe2 -N21	87.94(19)
N7 ² -Co2 -N15 ³	86.1(5)	C33-Fe2 -N23	92.65(19)
N7 ² -Co2 -N15	93.9(5)	C33-Fe2 -N21	92.4(2)
N16 ³ -Co2 -N7 ²	87.73(16)	C33-Fe2 -N19	177.9(2)
N16 -Co2 -N7 ¹	87.73(16)	C33-Fe2 -C32	88.1(2)
N16 ³ -Co2 -N7 ¹	92.27(16)	C31 -Fe2 -N23	177.7(2)
N16 -Co2 -N7 ²	92.27(16)	C31 -Fe2 -N21	91.1(2)
N16 ³ -Co2 -N16	180.0	C31 -Fe2 -N19	92.8(2)
N16 ³ -Co2 -N15	81.4(4)	C31 -Fe2 -C33	85.2(2)
N16 ³ -Co2 -N15 ³	98.6(4)	C31 -Fe2 -C32	89.3(2)
N16 -Co2 -N15 ³	81.4(4)	C32-Fe2 -N23	91.5(2)
N16 -Co2 -N15	98.6(4)	C32-Fe2 -N21	179.4(2)
N16 -Co2 -N15A ³	96.3(4)	C32-Fe2 -N19	91.6(2)
N16 ³ -Co2 -N15A ³	83.7(4)		
N16 -Co2 -N15A	83.7(4)		
N16 ³ -Co2 -N15A	96.3(4)		

N15-Co2-N15 ³	180.0(9)		
N15A ³ -Co2-N15A	180.0(5)		

Complex-1_desol			
Bond Length Å			
Co1-N9 ⁴	2.096(3)	Fe1-N1	1.979(3)
Co1-N9	2.096(3)	Fe1-N3	1.966(3)
Co1-N18 ⁵	2.137(3)	Fe1-N5	1.989(3)
Co1-N18 ⁶	2.137(3)	Fe1-C12	1.896(4)
Co1-N10	2.122(3)	Fe1-C10	1.916(4)
Co1-N10 ⁴	2.122(3)	Fe1-C11	1.924(4)
Co2-N7 ¹	2.120(3)	Fe2-N21	1.980(3)
Co2-N7 ²	2.120(3)	Fe2-N19	1.990(3)
Co2-N16	2.096(3)	Fe2-N23	1.978(3)
Co2-N16 ³	2.096(3)	Fe2-C33	1.914(4)
Co2-N15	2.133(3)	Fe2-C31	1.911(4)
Co2-N15 ³	2.133(3)	Fe2-C32	1.937(5)
Bond Angle (°)			
N10-Co1-N10 ¹	180.0	N1-Fe1-N5	87.75(12)
N10 ¹ -Co1-N18	90.55(11)	N3-Fe1-N5	87.75(12)
N10-Co1-N18	89.45(11)	N3-Fe1-N1	89.78(12)
N10 ¹ -Co1-N18 ¹	89.45(11)	C10-Fe1-N5	91.69(14)
N10-Co1-N18 ¹	90.55(11)	C10-Fe1-N1	92.93(14)
N9-Co1-N10	89.64(12)	C10-Fe1-N3	177.21(14)
N9 ¹ -Co1-N10	90.36(12)	C10-Fe1-C11	87.44(15)
N9-Co1-N10 ¹	90.36(12)	C11-Fe1-N5	179.11(15)
N9 ¹ -Co1-N10 ¹	89.64(12)	C11-Fe1-N1	92.16(14)
N9 ¹ -Co1-N9	180.0	C11-Fe1-N3	93.13(14)
N9-Co1-N18 ¹	88.70(11)	C12-Fe1-N5	90.93(14)
N9 ¹ -Co1-N18 ¹	91.30(11)	C12-Fe1-N1	177.90(15)
N9-Co1-N18	91.30(11)	C12-Fe1-N3	91.81(14)
N9 ¹ -Co1-N18	88.70(11)	C12-Fe1-C10	85.47(15)
N18-Co1-N18 ¹	180.00(4)	C12-Fe1-C11	89.13(15)
N7 ² -Co2-N7	180.0	N21-Fe2-N20	88.99(12)
N7-Co2-N15 ³	90.51(12)	N23-Fe2-N21	88.26(12)
N7-Co2-N15 ⁴	89.49(12)	N23-Fe2-N20	87.62(13)
N7 ² -Co2-N15 ⁴	90.51(12)	C31-Fe2-N21	177.27(14)
N7 ² -Co2-N15 ³	89.49(12)	C31-Fe2-N20	88.92(13)
N15 ³ -Co2-N15 ⁴	180.0	C31-Fe2-N23	89.90(15)
N16 ² -Co2-N7	88.26(12)	C31-Fe2-C33	85.50(14)
N16 ² -Co2-N7 ²	91.74(12)	C31-Fe2-C32	90.89(16)
N16-Co2-N7	91.74(12)	C33-Fe2-N21	96.54(13)
N16-Co2-N7 ²	88.26(12)	C33-Fe2-N20	174.25(13)
N16 ² -Co2-N15 ⁴	89.51(12)	C33-Fe2-N23	90.94(14)
N16 ² -Co2-N15 ³	90.49(12)	C33-Fe2-C32	89.72(16)
N16-Co2-N15 ³	89.52(12)	C32-Fe2-N21	90.93(14)
N16-Co2-N15 ⁴	90.48(12)	C32-Fe2-N20	91.80(14)
N16 ² -Co2-N16	180.0	C32-Fe2-N23	179.01(13)

Table S3. Average bond lengths (\AA) around Co and Fe centres at 103 K and 245 K of complex **1** \cdot 3.5H₂O

Bond	103 K	245 K
Co1-N	2.087(5)	2.111(4)
Co2-N	2.084(5)	2.126(4)
Fe1-C	1.906(6)	1.910(6)
Fe1-N	1.967(5)	1.971(4)
Fe2-C	1.919(6)	1.913(6)
Fe2-N	1.967(5)	1.968(5)

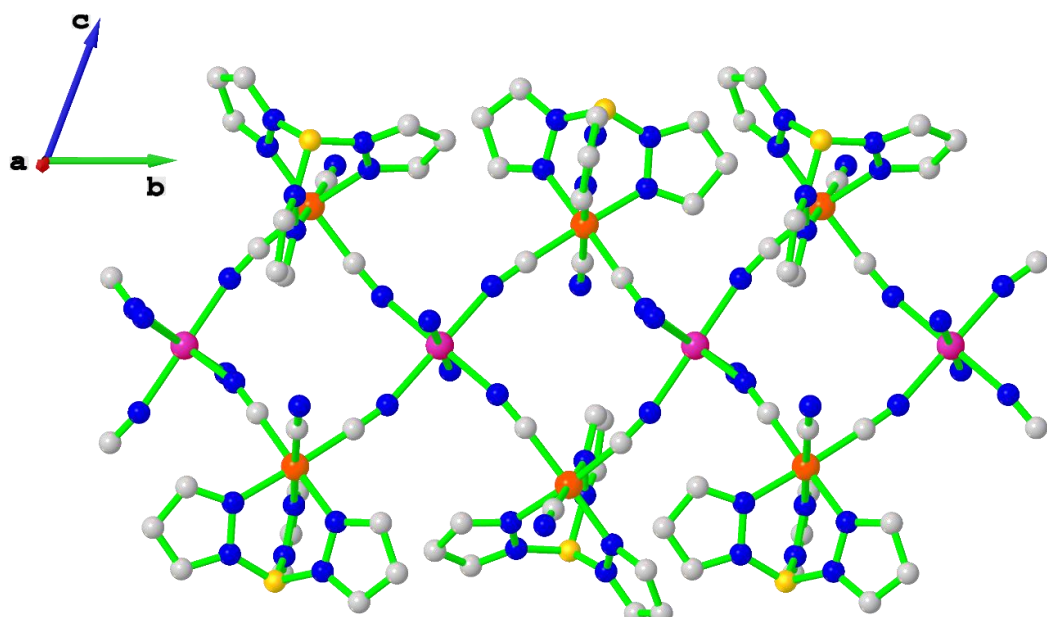


Figure S6. View of the 1D chain of $\{[\text{Fe}^{\text{III}}\text{Tp}(\text{CN})_3]_2[\text{Co}(\text{L}_2)]\}_n \cdot 3.5\text{H}_2\text{O}$ along the crystallographic a axis extending in the direction of b axis. Colour code: Fe (orange), Co (pink), C (grey), O (red) and N (blue).

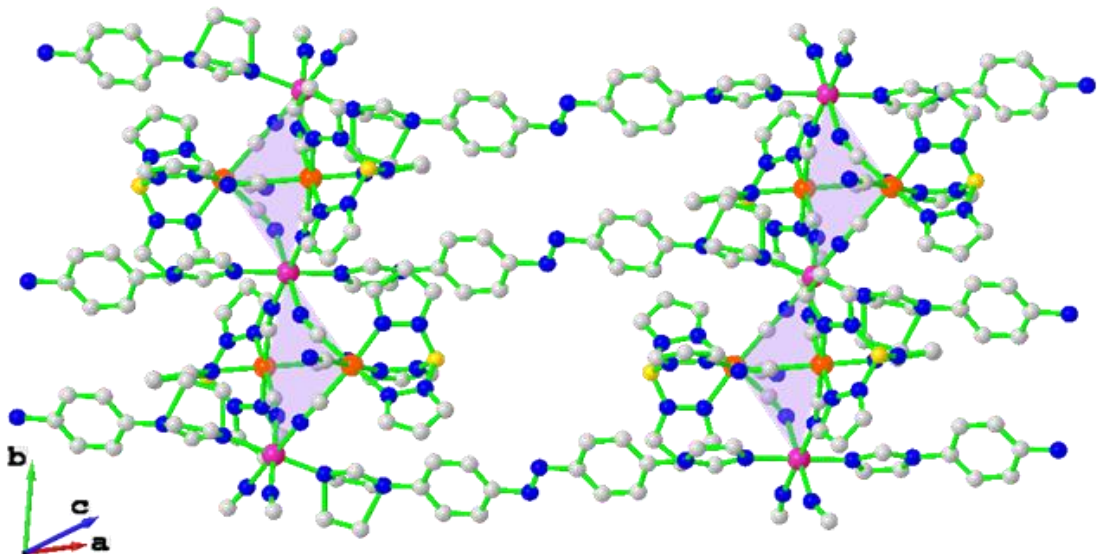


Figure S7. The 2D sheet of $\{[\text{Fe}^{\text{III}}\text{Tp}(\text{CN})_3]_2[\text{Co}(\text{L}_2)]\}_n \cdot 3.5\text{H}_2\text{O}$ formed by interlinking the 1D zig-zag chain structure along the a axis. Colour code: Fe (orange), Co (pink), C (grey), O (red) and N (blue).

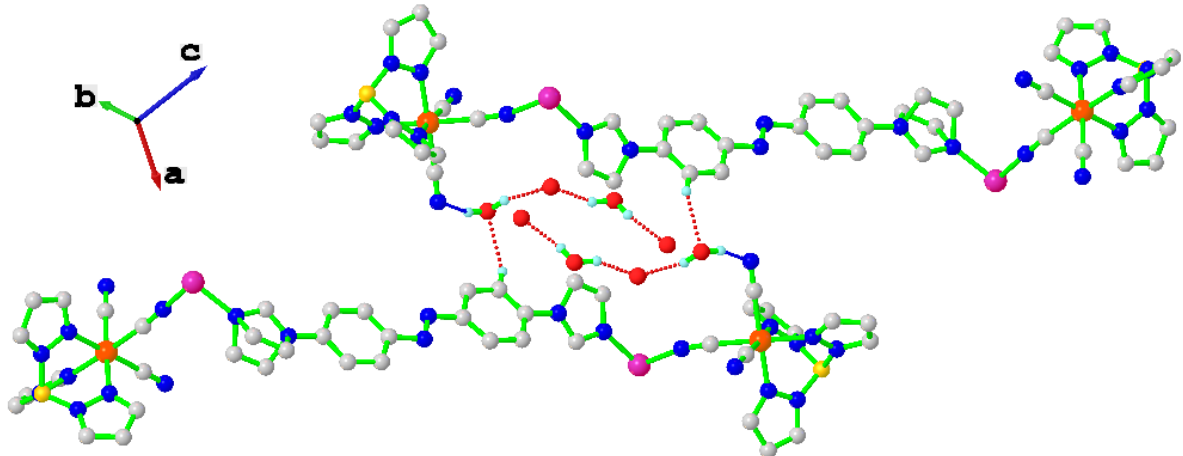


Figure S8. Hydrogen bonding interactions between the water molecules and terminal cyanide groups of $\{[\text{Fe}^{\text{III}}\text{Tp}(\text{CN})_3]\}_n$ units of $\{[\text{Fe}^{\text{III}}\text{Tp}(\text{CN})_3]_2[\text{Co}(\text{L}_2)]\}_n \cdot 3.5\text{H}_2\text{O}$ at 103 K. Colour code: Fe (orange), Co (pink), C (grey), O (red) and N (blue).

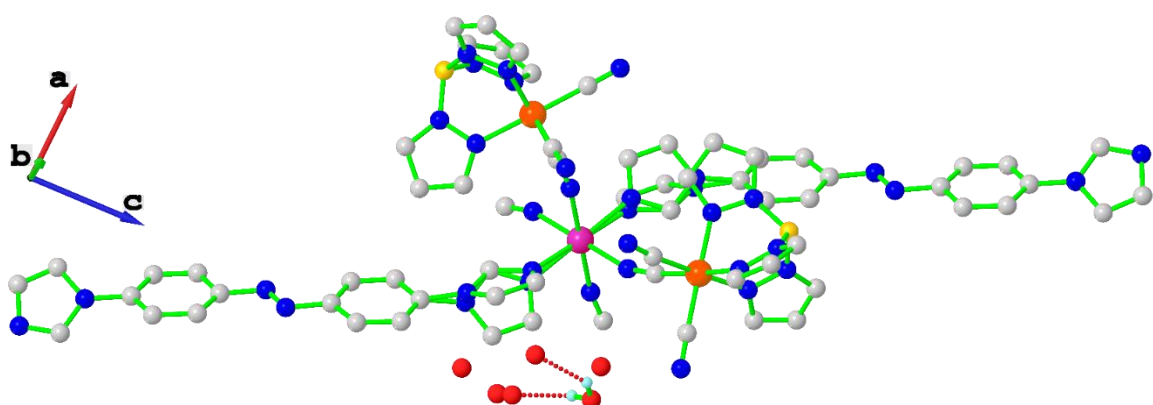


Figure S9. Hydrogen bonding interactions in the framework of $\{[\text{Fe}^{\text{III}}\text{Tp}(\text{CN})_3]_2[\text{Co}(\text{L}_2)]\}_n \cdot 3.5\text{H}_2\text{O}$ at 245 K. Colour code: Fe (orange), Co (pink), C (grey), O (red) and N (blue).

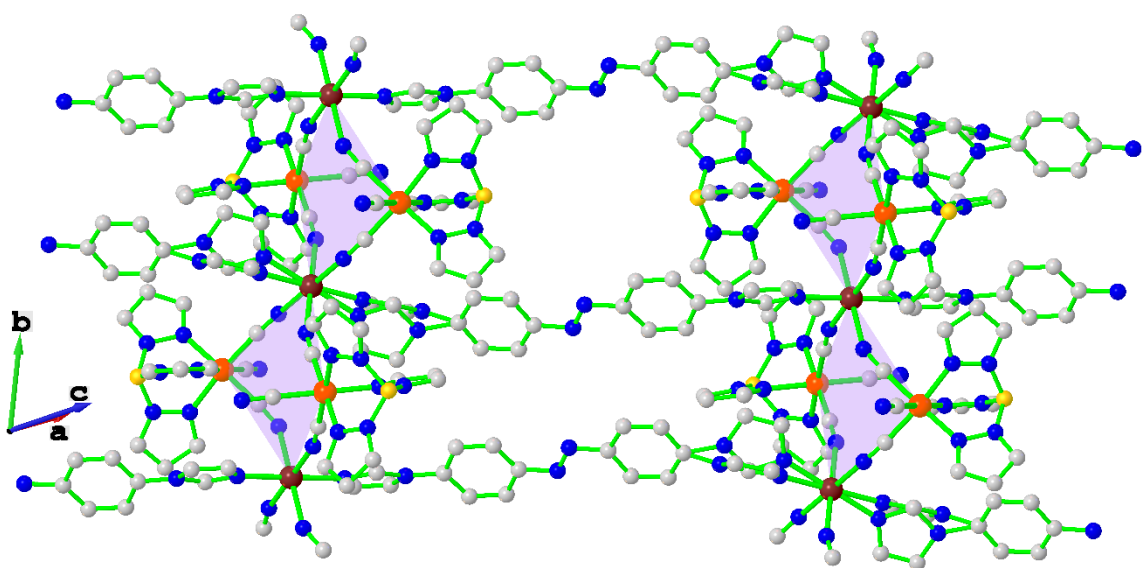


Figure S10. The 2D sheet of $\{[\text{Fe}^{\text{III}}\text{Tp}(\text{CN})_3]_2[\text{Zn}(\text{L}_2)]\}_n \cdot 3.5\text{H}_2\text{O}$ (**2**) formed by interlinking the 1D zig-zag chain structure along the a axis. Colour code: Fe (orange), Zn (maroon), C (grey), O (red) and N (blue).

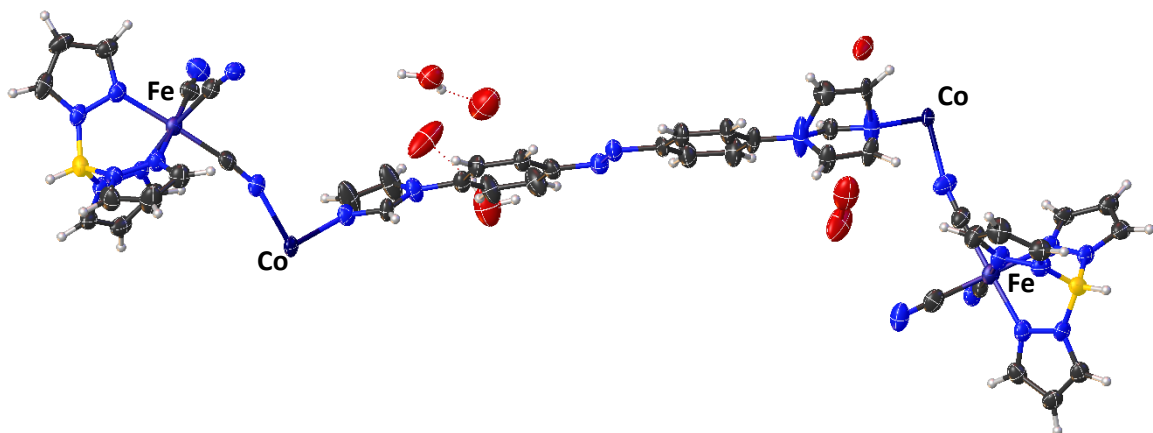


Figure S11. Thermal ellipsoid plot (50% probability) of $\{[\text{Fe}^{\text{III}}\text{Tp}(\text{CN})_3]_2[\text{Co}(\text{L}_2)]\}_n \cdot 3.5\text{H}_2\text{O}$ at 103 K. Colour code: Fe (blue), Co (dark blue), C (grey), O (red) and N (light blue).

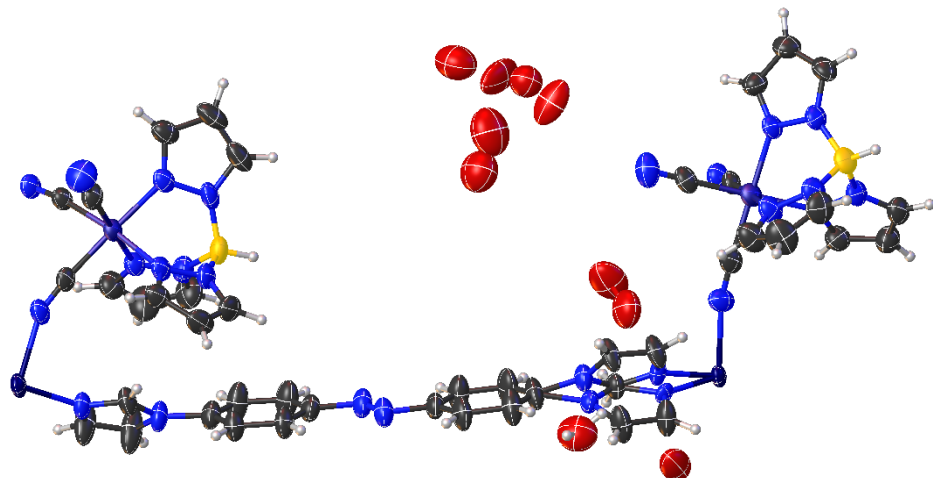


Figure S12. Thermal ellipsoid plot (50% probability) of $\{[\text{Fe}^{\text{III}}\text{Tp}(\text{CN})_3]_2[\text{Co}(\text{L}_2)]\}_n \cdot 3.5\text{H}_2\text{O}$ at 245 K. Colour code: Fe (blue), Co (dark blue), C (grey), O (red) and N (light blue).

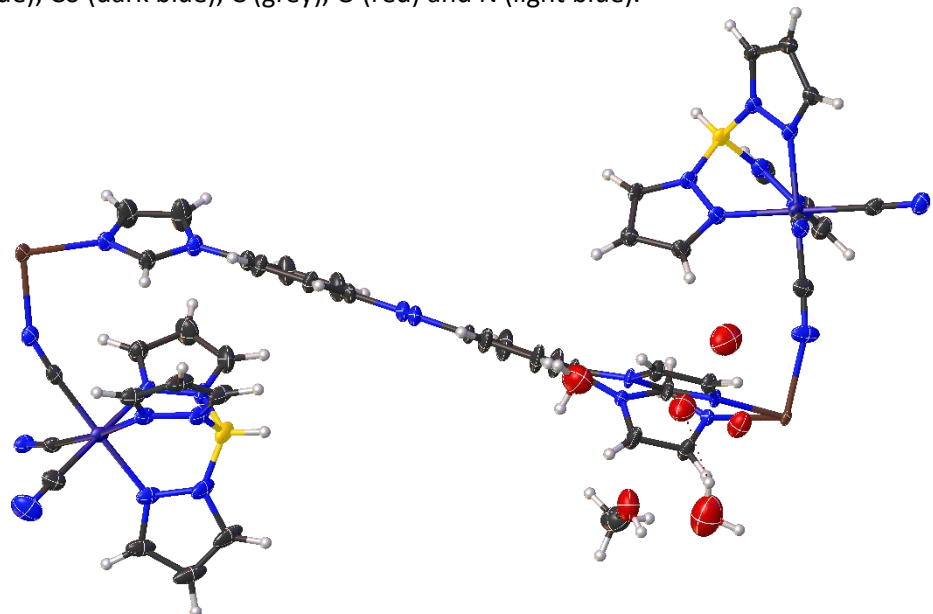


Figure S13. Thermal ellipsoid plot (50% probability) of $\{[\text{Fe}^{\text{III}}\text{Tp}(\text{CN})_3]_2[\text{Zn}(\text{L}_2)]\}_n \cdot 3.5\text{H}_2\text{O}$. Colour code: Fe (blue), Zn (brown), C (grey), O (red) and N (light blue).

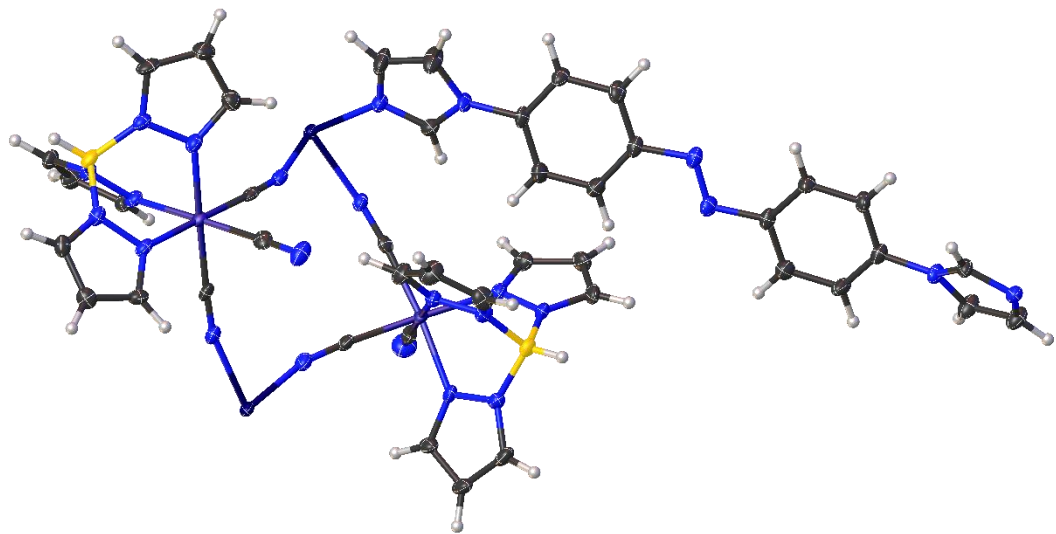


Figure S14. Thermal ellipsoid plot (50% probability) of $\{[\text{Fe}^{\text{III}}\text{Tp}(\text{CN})_3]_2[\text{Co}(\text{L}_2)]\}_n$ at 100 K. Colour code: Fe (blue), Co (dark blue), C (grey), O (red) and N (light blue). The absence of solvent molecules eliminates the disorder as indicated by the thermal ellipsoid as compared to S12 and S13

3.6. Mössbauer Studies:

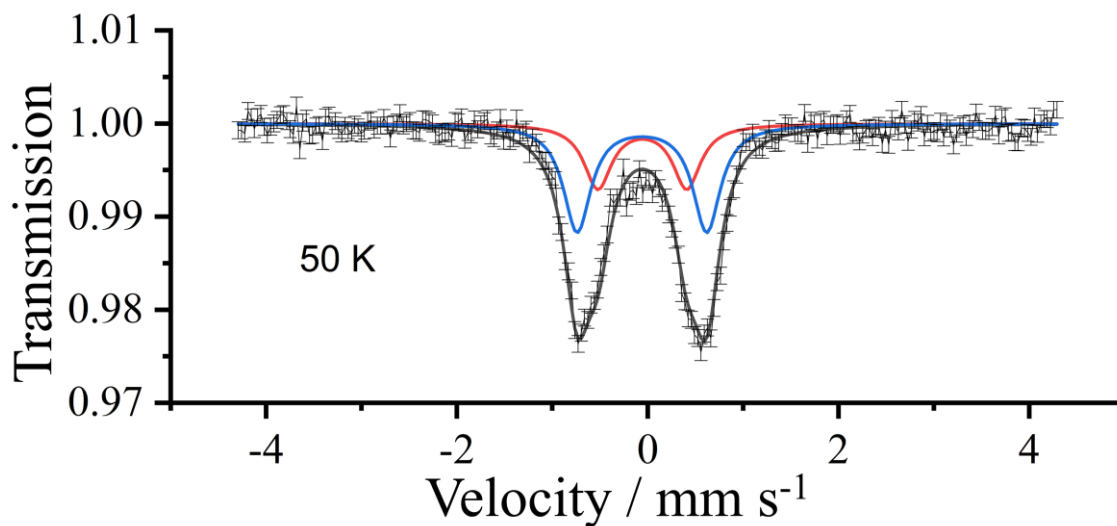


Figure S15. ^{57}Fe Mössbauer spectra at 50 K. Mössbauer parameters: $\delta = -0.06$ and $\Delta E_Q = 1.36 \text{ mm s}^{-1}$, corresponds to LS Fe^{III} ; $\delta = -0.06$ and $\Delta E_Q = 0.93 \text{ mm s}^{-1}$, corresponds to the LS Fe^{II} . The $\text{Fe}^{\text{III}}/\text{Fe}^{\text{II}}$ peak area ratio was 0.63/0.37, suggesting a mixture of $\{\text{Fe}^{\text{III}}_{\text{LS}}(\mu\text{-CN})\text{Co}^{\text{II}}_{\text{HS}}(\mu\text{-NC})\text{Fe}^{\text{III}}_{\text{LS}}\}$ and $\{\text{Fe}^{\text{II}}_{\text{LS}}(\mu\text{-CN})\text{Co}^{\text{III}}_{\text{LS}}(\mu\text{-NC})\text{Fe}^{\text{III}}_{\text{LS}}\}$ linkages. The solid lines are Lorentzian curves plotted by the calculated values. The Mössbauer studies was performed on the product obtained via direct mixing of the reactant which exhibit higher extent of magnetic transition than the crystal product obtained by slow diffusion technique (Fig S19).

3.7. Shape Analysis:

Table S4. Summary of SHAPE analysis around Co in complex **1·3.5H₂O** at 103K

				Co1	Co2
1.	HP-6	D6h	Hexagon	32.406	31.658
2.	PPY-6	C5v	Pentagonal pyramid	29.919	29.498
3.	OC-6	Oh	Octahedron	0.013	0.057
4.	TPR-6	D3h	Trigonal prism	16.553	16.371
5.	JPPY-6	C5v	Johnson pentagonal pyramid J2	33.400	32.882

Table S5. Summary of SHAPE analysis around Co in complex **1·3.5H₂O** at 245 K

				Co1	Co2
1.	HP-6	D6h	Hexagon	32.543	29.276
2.	PPY-6	C5v	Pentagonal pyramid	29.970	28.404
3.	OC-6	Oh	Octahedron	0.014	0.256
4.	TPR-6	D3h	Trigonal prism	16.556	16.180
5.	JPPY-6	C5v	Johnson pentagonal pyramid J2	33.451	31.581

Table S6. Summary of SHAPE analysis around Co in complex **1** at 100 K

				Co1	Co2
1.	HP-6	D6h	Hexagon	32.479	32.671
2.	PPY-6	C5v	Pentagonal pyramid	29.859	29.956
3.	OC-6	Oh	Octahedron	0.018	0.023
4.	TPR-6	D3h	Trigonal prism	16.572	16.436
5.	JPPY-6	C5v	Johnson pentagonal pyramid J2	33.289	33.392

Table S7. The fit parameters for the linear fitting of $\ln(\tau)$ vs. T^{-1} for complex **1·3.5H₂O** and **1**

Complex	1·3.5H₂O	1
Equation	$y = a + b*x$	$y = a + b*x$
Intercept	-17.3628 ± 0.28976	-18.35451 ± 0.78307
Slope	34.89463 ± 0.88176	32.61178 ± 1.96253
Residual Sum of Squares	0.02482	0.52351
Pearson's r	0.99873	0.99107
R-Square (COD)	0.99745	0.98221
Adj. R-Square	0.99682	0.97866

Table S8. The fit parameters for the linear fitting of $\ln(\chi'T)$ vs. T^{-1} for complex **1·3.5H₂O** and **1**

Complex	1·3.5H₂O	1
Equation	$y = a + b*x$	$y = a + b*x$
Intercept	1.62452 ± 0.01309	2.10389 ± 0.0151
Slope	22.27239 ± 0.1708	23.16861 ± 0.16998
Residual Sum of Squares	0.04043	0.01782
Pearson's r	0.99827	0.9993
R-Square (COD)	0.99654	0.9986
Adj. R-Square	0.99648	0.99855

Table S9. Fe-Co based SCMs exhibiting ETCST phenomenon

Compound	Stimuli for ETCST	Ref.
{[Fe(pzTp)(CN) ₃] ₂ Co(4-styrylpyridine) ₂ } · 2H ₂ O · 2CH ₃ OH	Light	9
{[Fe(bpy)(CN) ₄] ₂ Co(4,4'-bipyridine)} · 4H ₂ O	Light	10
{[Fe(bpy)(CN) ₄] ₂ Co(phpy) ₂ } · 2H ₂ O	Light	11
[Co((R)-pabn)][Fe(Tp)(CN) ₃](BF ₄) · H ₂ O	Light	12
{[Fe(bipy)(CN) ₄] ₂ [Co(phpy) ₂]}	Dehydration	13
{[Fe ^{III} (bipy)(CN) ₄] ₂ Co ^{II} (2,4' -bpy) ₂ }	Light	14
{[pzTpFe(CN) ₃] ₄ Co ₂ (Bib) ₄ } · 3H ₂ O	Light	15
{[pzTpFe(CN) ₃] ₂ Co(Bpi) ₂ } · CH ₃ CN · 4H ₂ O	Light	15
{[(PzTp)Fe(CN) ₃] ₂ Co(L) ₂ } · 4H ₂ O	Light	16
{[(Tp)Fe(CN) ₃] ₂ Co(L) ₂ } · 3H ₂ O · CH ₃ OH	Light	16
{[(Tp)Fe(CN) ₃] ₂ Co(BIT)} · 2CH ₃ OH	Light	17

L: (4-(1H-imidazol-5-ylmethylene-amino)-4H-1,2,4-triazole; Phpy: Phenyl pyridine; Bib: 1,4-bis-(1H-imidazol-1-yl)benzene); Bpi: 1-Biphenyl-4-yl-1H-imidazole; BIT: 3,4-bis-(1H-imidazol-1-yl)thiophen

3.8. Thermogravimetric Analysis (TGA):

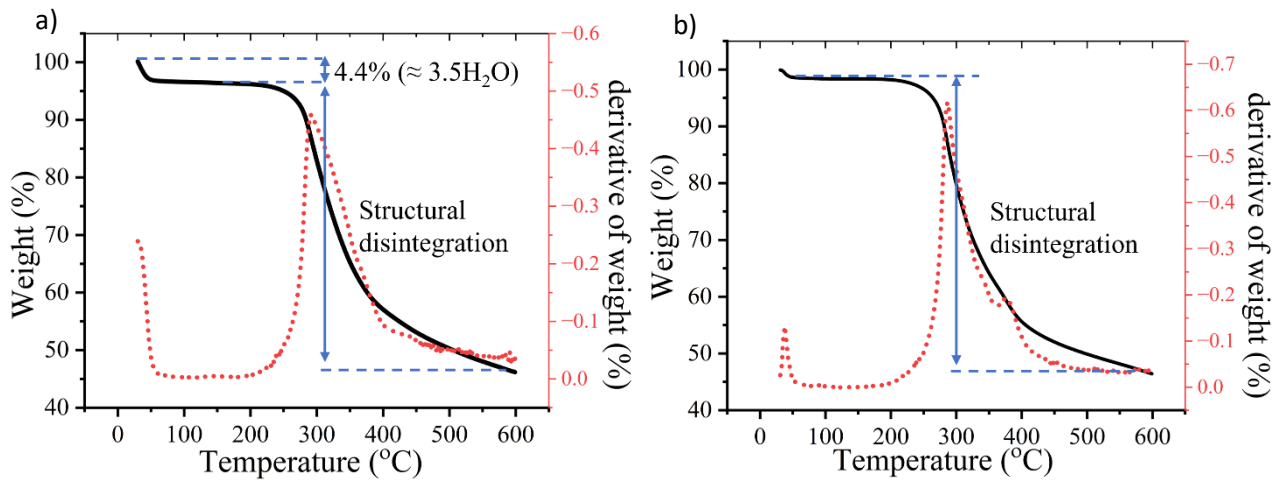


Figure S16. a) TGA of **1·3.5H₂O** depicting the solvent loss from 30 °C onwards which approximately accounts for the loss of 3.5H₂O. b) TGA of **1** disintegrates above 250 °C representing a negligible loss which might be due to the moisture present on the sample surface. In both the cases the molecule

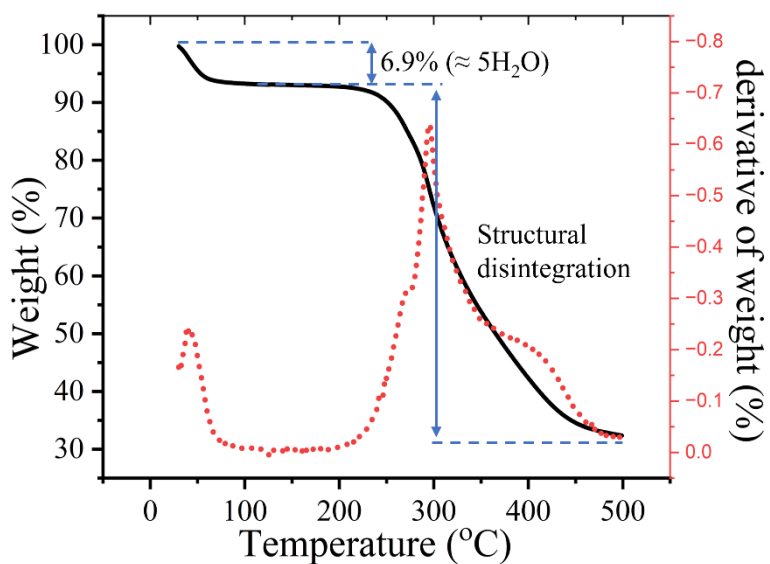


Figure S17. TGA of the sample prepared by direct mixing. The compound rapidly loses solvent molecules indicating the loss of approximately 5 H₂O molecules. The loss above 250 °C indicates structural disintegration

3.9. Magnetic data:

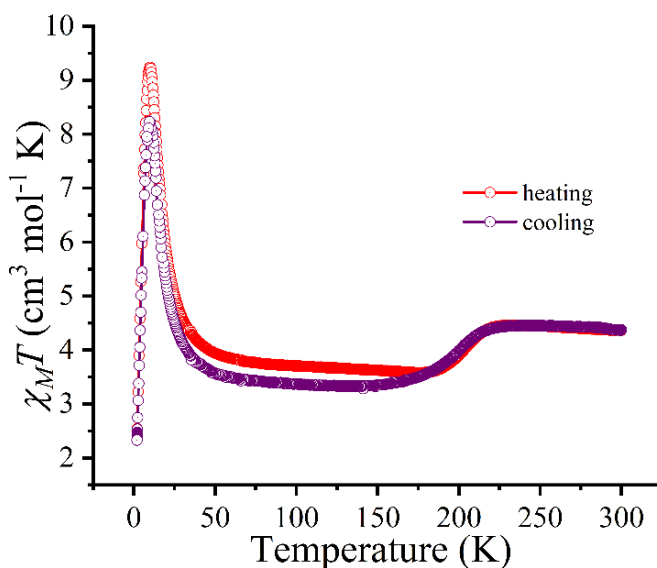


Figure S18. $\chi_M T$ vs T plot for heating (2 to 300 K) and cooling (300 to 2 K) mode for complex **1·3.5H₂O**.

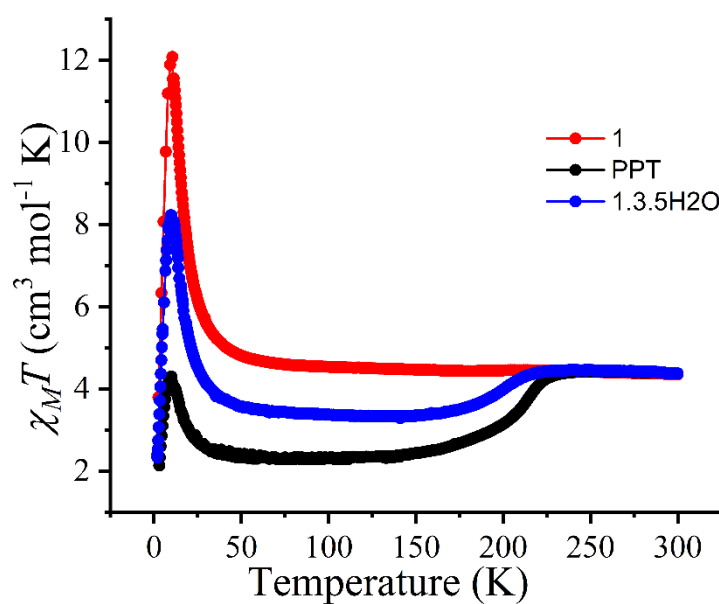


Figure S19. $\chi_M T$ vs T plot for complexes **1·5H₂O** (black), **1** (red) and **1·3.5H₂O** (blue) in 2-300 K range

The amount of the H₂O molecules is directly affecting the fraction of the molecule undergoing ETCST phenomenon. The sample prepared by direct mixing exhibited higher extent of ETCST behaviour, while the transition temperature remains same. TGA analysis revealed that the weight loss corresponds to five H₂O molecules corresponding the sample to be **1·5H₂O** (Fig S17). The fractional conversion for **1·5H₂O** correlates with the Mössbauer data (Fig S15).

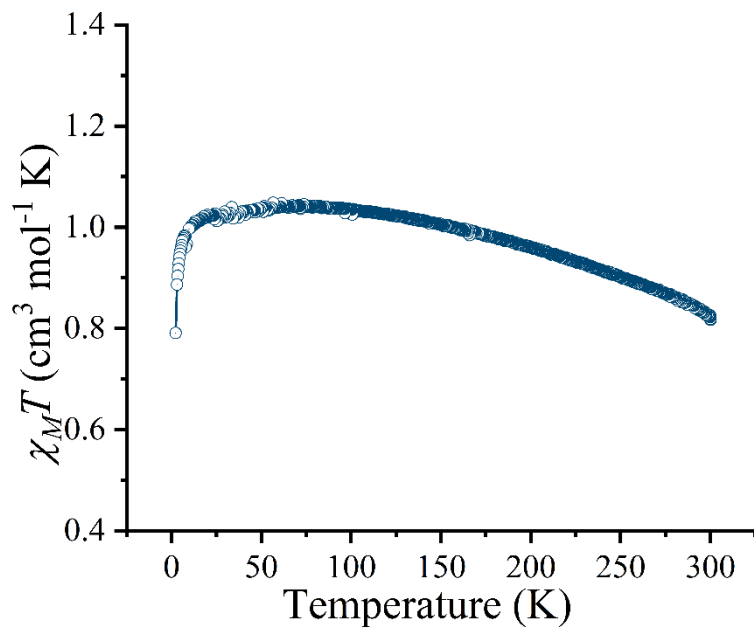


Figure S20. $\chi_M T$ vs T plot indicating the absence of ETCST in complex **2**.

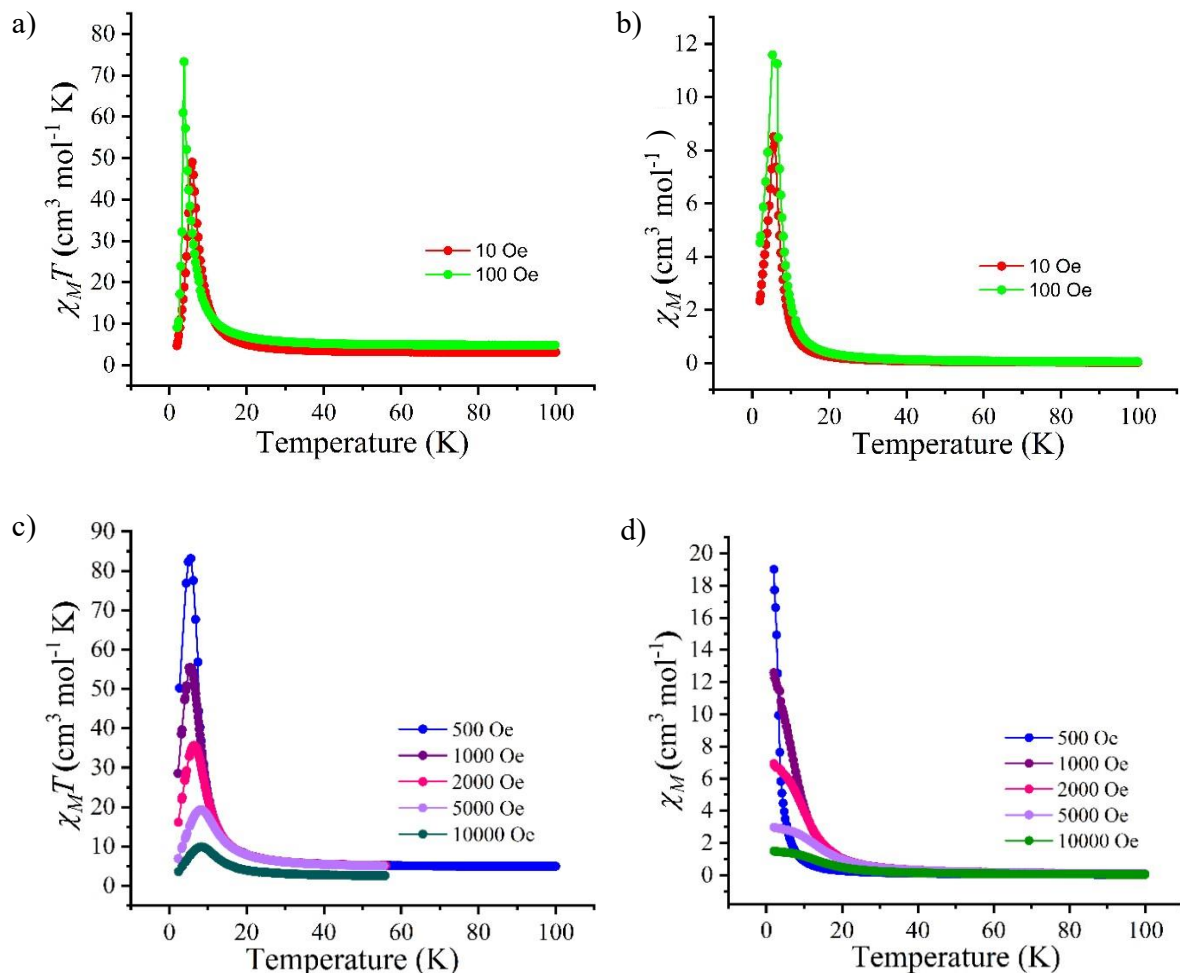


Figure S21. Low-temperature behaviour of χ_M vs T and $\chi_M T$ vs T as a function of applied field for complex **1**·3.5H₂O.

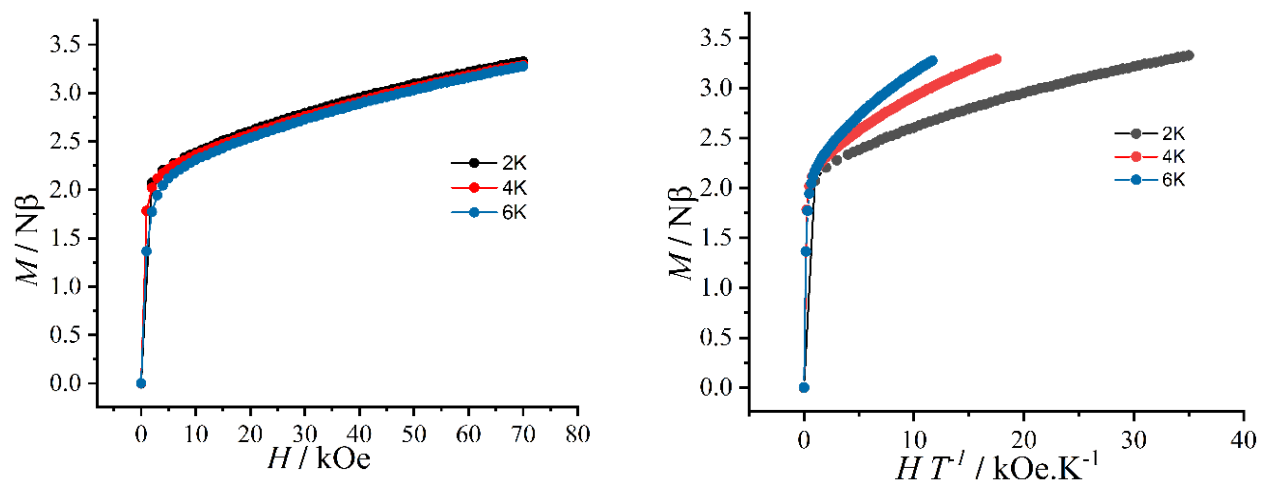


Figure S22. Magnetization vs magnetic field (left) and reduced magnetization (right) plots for complex **1**·3.5H₂O.

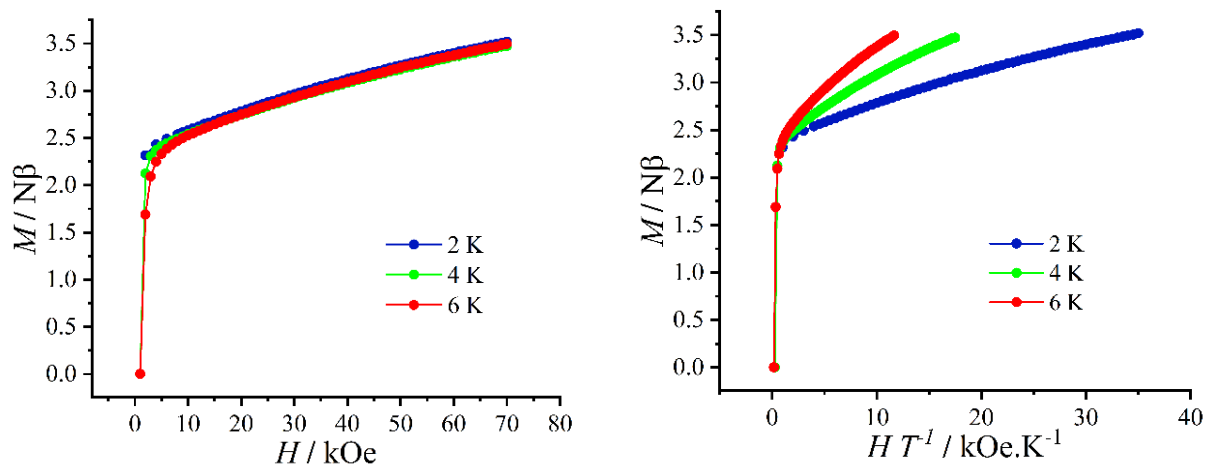


Figure S23. a) Magnetization vs magnetic field and b) reduced magnetization plots for complex **1**.

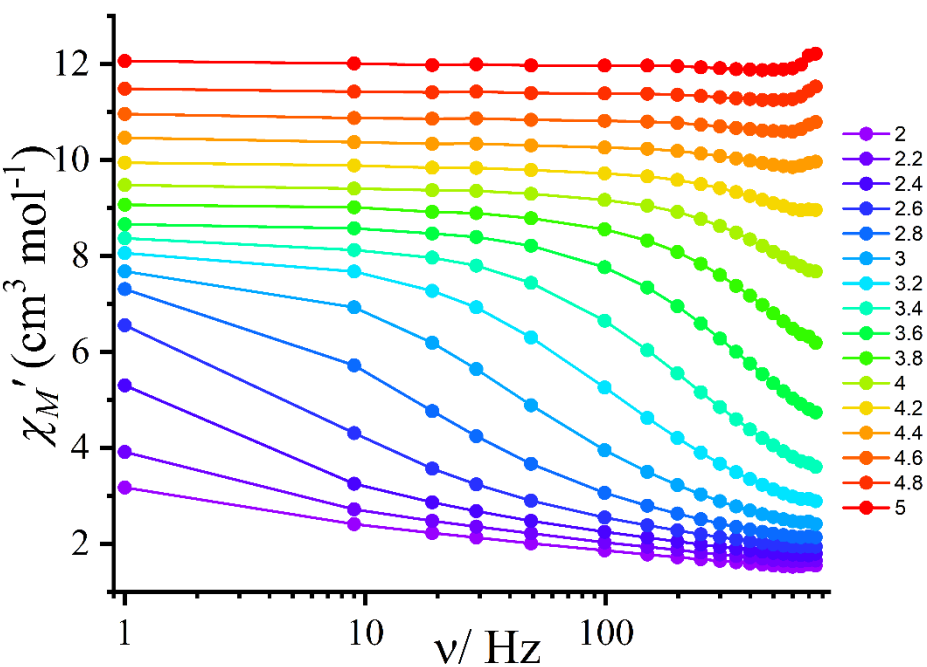


Figure S24. Variable-frequency in-phase (χ') ac magnetic susceptibility data for **1·3.5H₂O** collected in a 3.5 Oe ac field (Hac) and dc field of 0 Oe (Hdc)

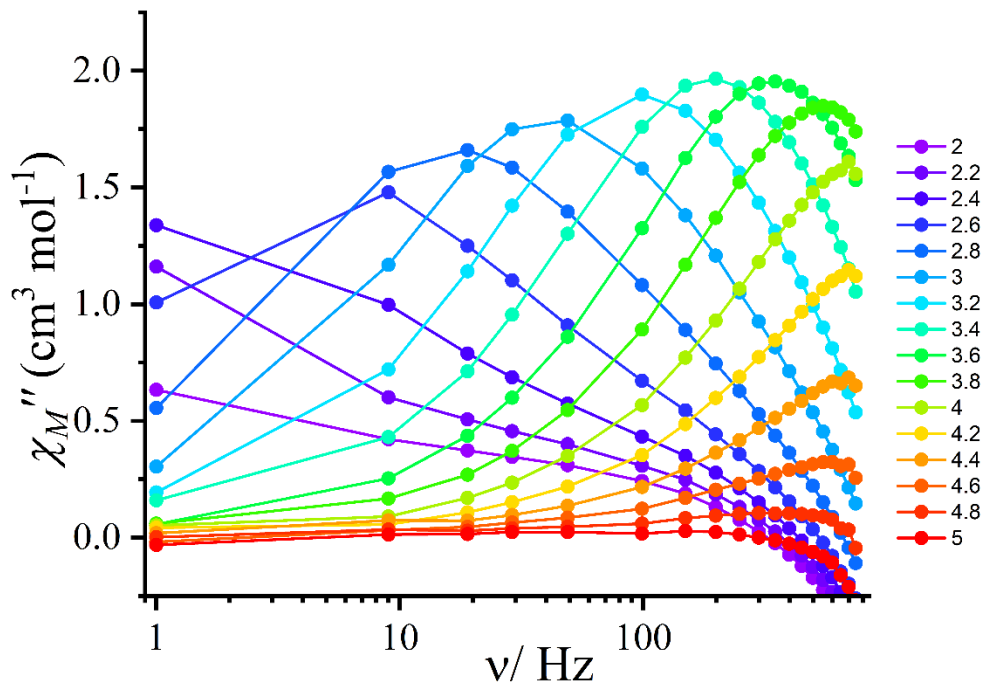


Figure S25. Variable-frequency out-of-phase (χ'') ac magnetic susceptibility data for **1·3.5H₂O** collected in a 3.5 Oe ac field (Hac) and dc field of 0 Oe (Hdc)

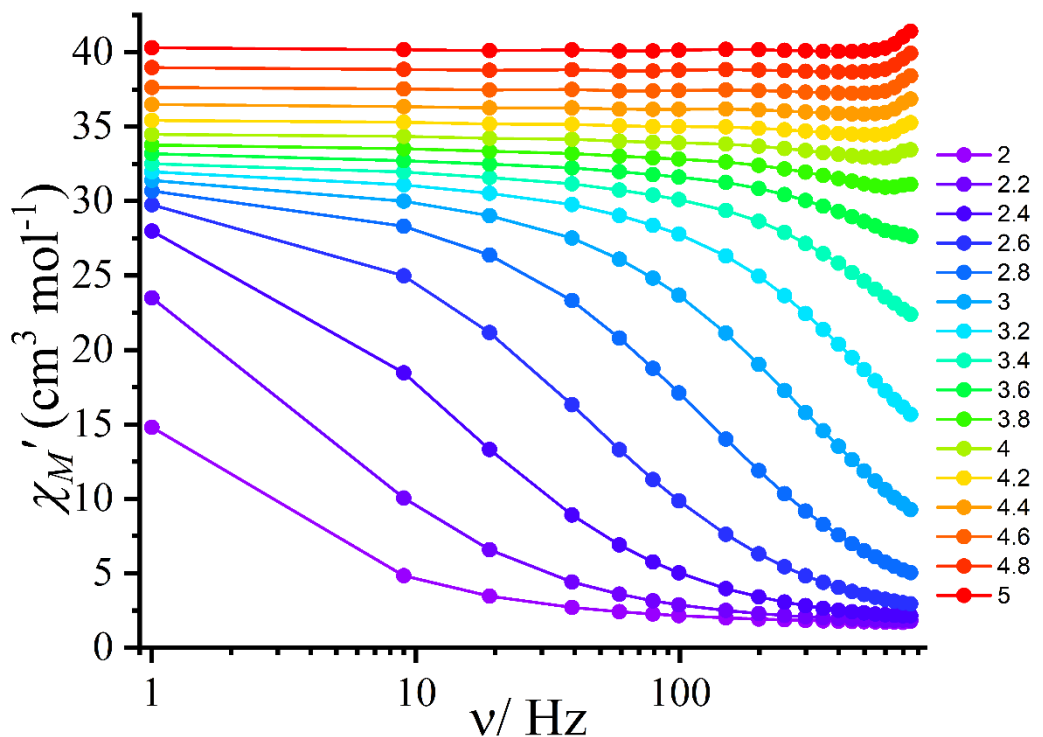


Figure S26. Variable-frequency in-phase (χ') ac magnetic susceptibility data for **1** collected in a 3.5 Oe ac field (Hac) and dc field of 0 Oe (Hdc)

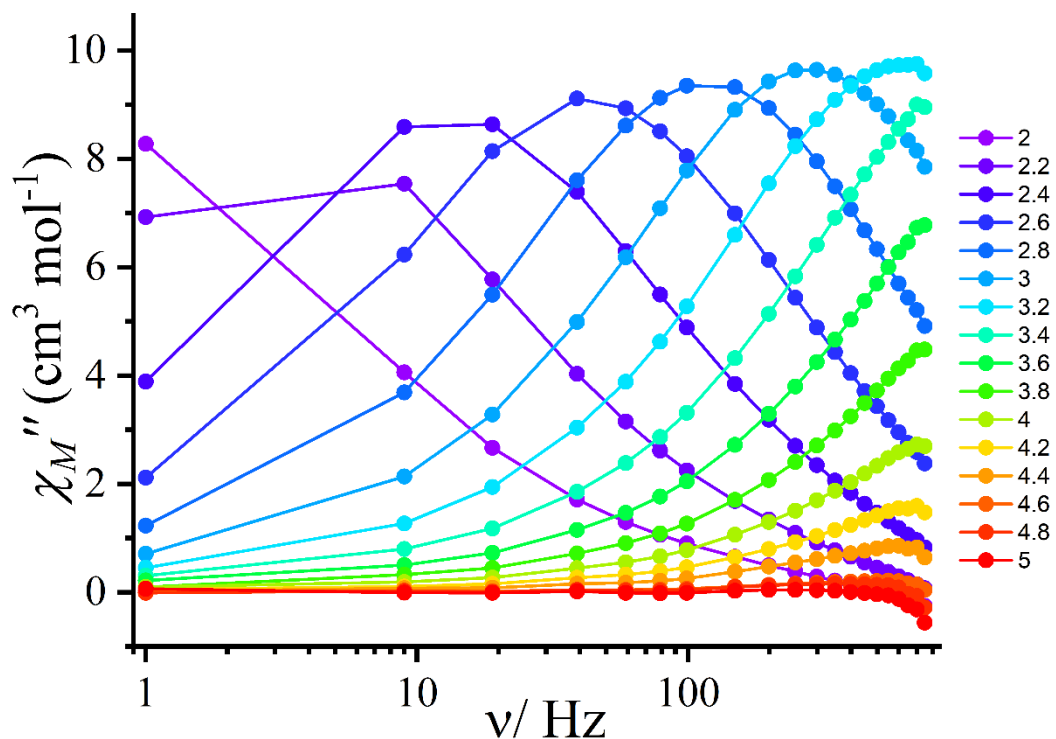


Figure S27. Variable-frequency out-of-phase (χ'') ac magnetic susceptibility data for **1** collected in a 3.5 Oe ac field (Hac) and dc field of 0 Oe (Hdc)

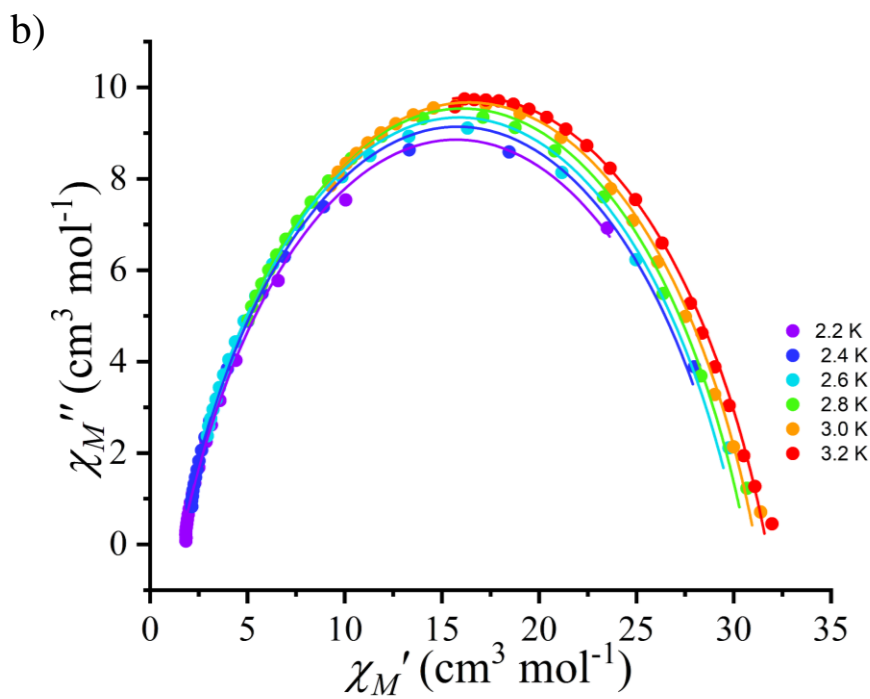
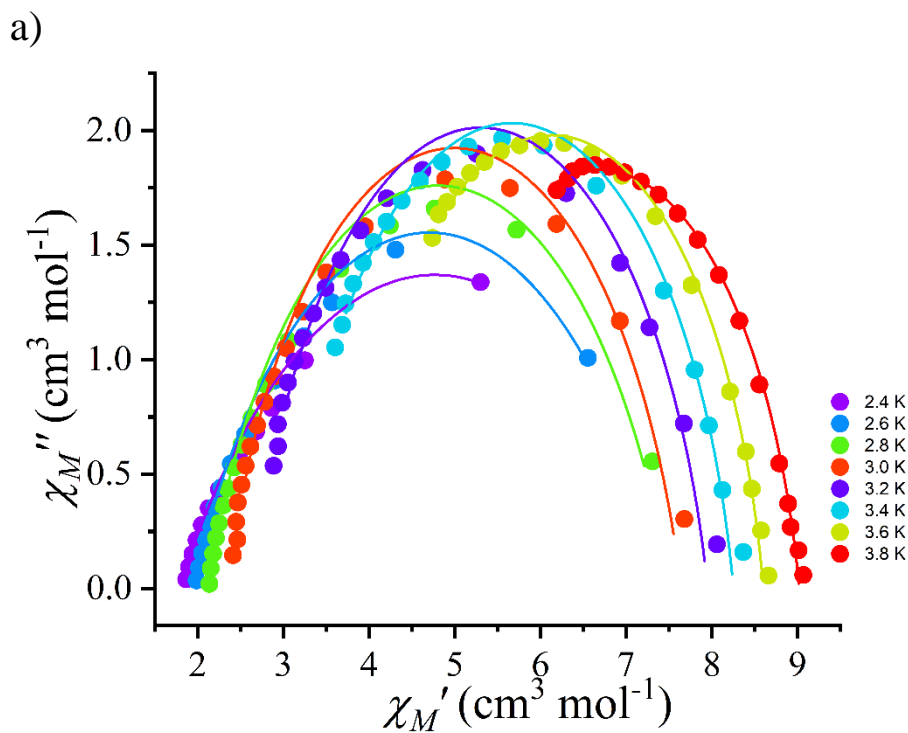


Figure S28. Cole–Cole plots of **1**·3.5H₂O (a) and **1** (b); the solid lines are least-square fittings for a distribution of single relaxation processes using generalized Debye model with α ranging from 0.14 to 0.45 and 0.26 to 0.28 for **1**·3.5H₂O and **1** respectively.

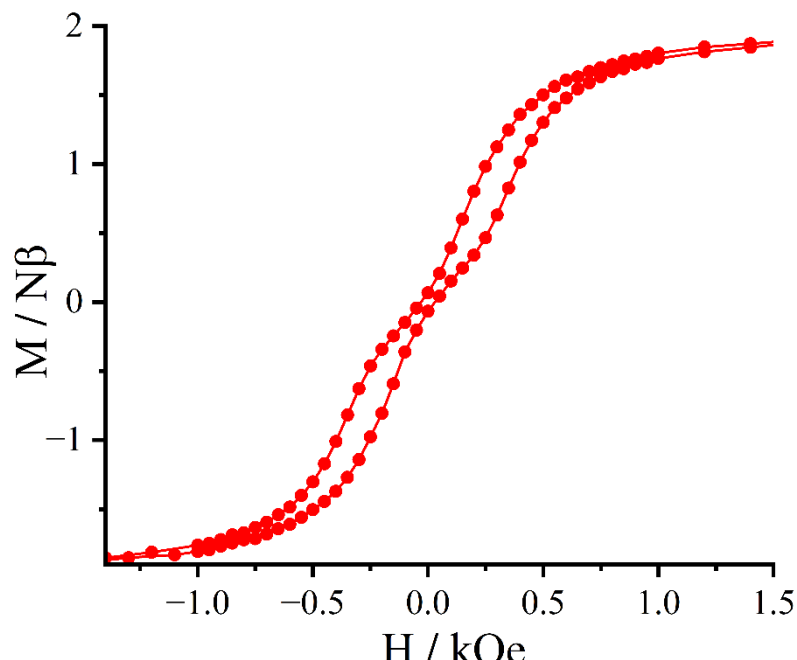


Figure S29. a) Hysteresis observed in the magnetization vs. magnetic field plot in a field sweep rate of 100 Oe per minute for complex **1·3.5H₂O**.

References:

1. J. Kim, S. Han, I.-K. Cho, K. Y. Choi, M. Heu, S. Yoon and B. J. Suh, *Polyhedron*, 2004, **23**, 1333-1339.
2. J. Yadav, D. J. Mondal and S. Konar, *Chem. Commun.*, 2021, **57**, 5925-5928.
3. P. Mondal, B. Dey, S. Roy, S. P. Bera, R. Nasani, A. Santra and S. Konar, *Crystal Growth & Design*, 2018, **18**, 6211-6220.
4. M. K. Sharma and P. K. Bharadwaj, *Inorg. Chem.*, 2011, **50**, 1889-1897.
5. SAINT, Data Reduction and Frame Integration Program for the CCD Area-Detector System. Bruker Analytical X-ray Systems, Madison, Wisconsin, USA, 1997-2006.
6. G.M. Sheldrick, SADABS, Program for Area Detector Adsorption Correction, Institute for Inorganic Chemistry, University of Göttingen, Germany, 1996.
7. O. V. Dolomanov, L. J. Bourhis, R. J. Gildea, J. A. K. Howard and H. Puschmann, *Journal of Applied Crystallography*, 2009, **42**, 339-341.
8. G. Sheldrick, *Acta Crystallographica Section A*, 2015, **71**, 3-8.
9. D. P. Dong, T. Liu, S. Kanegawa, S. Kang, O. Sato, C. He and C. Y. Duan, *Angew. Chem. Int.Ed.*, 2012, **51**, 5119-5123.
10. T. Liu, Y.-J. Zhang, S. Kanegawa and O. Sato, *J. Am. Chem. Soc.*, 2010, **132**, 8250-8251.
11. W. Jiang, C. Jiao, Y. Meng, L. Zhao, Q. Liu and T. Liu, *Chem. Sci.*, 2018, **9**, 617-622.

12. N. Hoshino, F. Iijima, G. N. Newton, N. Yoshida, T. Shiga, H. Nojiri, A. Nakao, R. Kumai, Y. Murakami and H. Oshio, *Nat. Chem.*, 2012, **4**, 921-926.
13. W. J. Jiang, H. H. Lu, Y. S. Meng, C. Q. Jiao and T. Liu, *Inorg. Chem. Commun.*, 2020, **112**, 107715.
14. Z. Shao, W. J. Jiang, L. Zhao, D. Liu, Y. S. Meng and T. Liu, *Inorg. Chem. Commun.*, 2023, **153**, 110727.
15. J. X. Hu, H. L. Zhu, Y. S. Meng, J. Pang, N. Li, T. Liu and X. H. Bu, *CCS. Chem.*, 2023, **5**, 865-875.
16. Q. Liu, N. T. Yao, H. Y. Sun, J. X. Hu, Y. S. Meng and T. Liu, *Inorg. Chem. Front.*, 2022, **9**, 5093-5104.
17. N.-T. Yao, L. Zhao, C. Yi, Q. Liu, Y.-M. Li, Y.-S. Meng, H. Oshio and T. Liu, *Angew. Chem. Int. Ed.*, 2022, **61**, e202115367.